# RADAR TRACKING AND OBSERVATION OF NONCOOPERATIVE SPACE OBJECTS BY REENTRY OF SALYUT-7/KOSMOS-1686

D. Mehrholz, K. Magura

Research Establishment for Applied Science (FGAN)
Research Institute for High Frequency Physics (FHP)

ABSTRACT

Radar observations of the decayed USSR space station SALYUT-7/KOSMOS-1686 have been frequently performed by FGAN-FHP since 1990. Main objective was to support and advise the German government in all matters concerned with the reentry. Narrowband as well as high resolution radar data have been analysed to assist reentry predictions at FGAN-FHP and at ESA-ESOC.
The paper provides background information to FGAN-FHP experimental radar research related to low earth orbit. The concept of the high resolution radar is discussed. Methods to determine physical characteristics like size, shape, and intrinsic motion of non-cooperative space objects are highlighted. Results achieved from SALYUT-7/KOSMOS-1686 reentry observations are shown.

Keywords: Radar observation of space objects, tracking radar, imaging radar, range-Doppler imaging, SALYUT-7/KOSMOS-1686 reentry.

## 1. BACKGROUND

### 1.1 Research Areas and Objectives

With regard to low earth orbit (LEO) FGAN-FHP is concerned with research in the following areas:

- Decay predictions of high risk space objects.
  By definition high risk space objects are those satellites which do have a mass of more then 12.000 kg or satellites which carry nuclear material on board. The aim is to support and advise the German government in all matters concerned with the decay: lifetime prediction, time-window and decay-area estimation, and risk assessment. The responsibility is at the Federal Ministry of Interior (BMI). In cases where the satellite carries nuclear material the Federal Ministry for the Environment Nature Conservation and Nuclear Safety (BMU) is also involved.
- Physical characteristics of space debris.
  Explosions and collisions in space are the major sources of orbital debris. The fragments pose a hazard especially to large spacecraft planned to operate for long periods of time. There is little known about true physical characteristics (size, shape, intrinsic motion, and mass) of larger orbital debris. Objective of a scientific cooperation between NASA and FGAN-FHP is to derive physical characteristics from narrowband and high resolution radar data.
- Determination of spacecraft parameters.
  The mathematical modelling of satellite trajectories which are perturbed by aerodynamic forces is an important task: For orbit prediction of decaying space objects, for long-term as well as short-term lifetime estimation, and for mass assessment. A scientific cooperation between ESA-ESOC, Hyperschall Technologie Göttingen (HTG), DLR Göttingen, and FGAN-FHP led to the development of sets of computer assisted tools and procedures to determine drag and lift of those satellites for which size, shape, and intrinsic motion are fairly good known.

Main objectives in these research areas are investigation of methods for:

- orbit analysis,
- determination of spacecraft size and shape,
- estimation of spacecraft attitude,
- orbital lifetime prediction, and
- spacecraft mass assessment.

In order to perform research in the areas mentioned before the following systems and analysis tools have been developed:

- Experimental radar system.
  The system consists of a L-band tracking radar, and a Ku-band imaging radar. Both radars are supported by a 34-m-antenna.
- Software for orbit determination and prediction.
  Orbit computation is based on the theory of Brouwer and Lyddane. This analytical solution of drag-free satellite motion allows fast realtime prediction of satellite orbits for radar system control. The influence of air drag is taken into account by assuming the mean motion as a linear function of time. After a satellite passage the radar data are used to determine new mean orbital elements. There

are also programs available which predict and determine satellite orbits by numerical integration of the motion equations.

- Software for mass assessment.
  The ballistic coefficient is estimated from the first derivative of the mean motion and by using the CIRA-72 air density model. The derivative of the mean motion is computed from the time history of NASA 2-line-elements as well as from FGAN-FHP radar data.
  In cases where sufficient information regarding the average reference area (shape, size, and motion) and the drag coefficient is available the mass of a satellite can be computed. Knowledge of shape, size, and motion are gained from analysis of FGAN-FHP narrowband and broadband radar data.
  The accuracy of mass assessments is in the order of 10% to 20%.
- Software for lifetime prediction.
  Satellite orbital lifetime is predicted at FGAN-FHP by use of a computer assisted approach based on a method of King-Hele. The method is analytical, it depends on an approximated solution of the Lagrange planetary equations for the semi major axis and the eccentricity. The accuracy for short-term and medium-term predictions is said to be ±10% of the estimated lifetime with the assumption that:
  - stabilization, and
  - configuration does not change,
  - no manoeuvre, and
  - no abnormal development of the density parameters of the high atmosphere will happen.

  At present the necessary information is taken from NASA 2-line-elements or computed from FGAN-FHP radar data. The parameters of interest are the revolutions per day as well as its first and second derivatives. In addition the development of the solar activity (and thereby the air density) is estimated based on the history of the 10.7 cm solar flux data and the geomagnetic activity.
- Software for narrowband signature analysis.
  Various noncoherent and coherent signature analysis methods have been developed and are in use.
- Software for computation of radar images.
  The most efficient imaging method used at FGAN-FHP is based on the range-Doppler imaging (RDI) principle.

## 1.2 SALYUT-7/KOSMOS-1686 Observation Scenario

The typically daily observation scenario using a ground based station (e.g. FGAN-FHP radar site) is shown in a polar plot (Fig. 1.2.1) for the soviet space station SALYUT-7/KOSMOS-1686. Most of the subtracks are in the southern region since the inclination of the satellite orbit is not much larger then the geographical latitude of the radar site.

For the last twenty days before the decay Fig. 1.2.2 shows all passages of the space station which could be observed from the FGAN-FHP radar site. It is evident that only 5 to 6 passages daily are within the line of sight (LOS). Each observation interval is about 6 minutes. After 5 to 6 consecutive passages the object is outside LOS for about 16 hours.

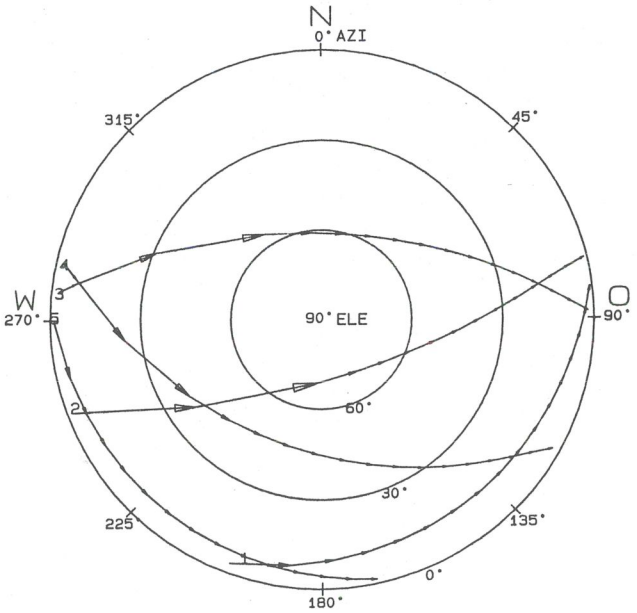


| passage No. | start (UTC) YY:DD:HH:MM | end YY:DD:HH:MM |
|---|---|---|
| 1 | 91:30:07:44 | 91:30:07:50 |
| 2 | 91:30:09:16 | 91:30:09:23 |
| 3 | 91:30:10:48 | 91:30:10:55 |
| 4 | 91:30:12:21 | 91:30:12:27 |
| 5 | 91:30:13:53 | 91:30:13:59 |

Fig.1.2.1: Polar plot and table of observable passages of SALYUT-7/KOSMOS-1686 on 30 Jan. 91, computed for the FGAN-FHP radar at Wachtberg-Werthhoven.

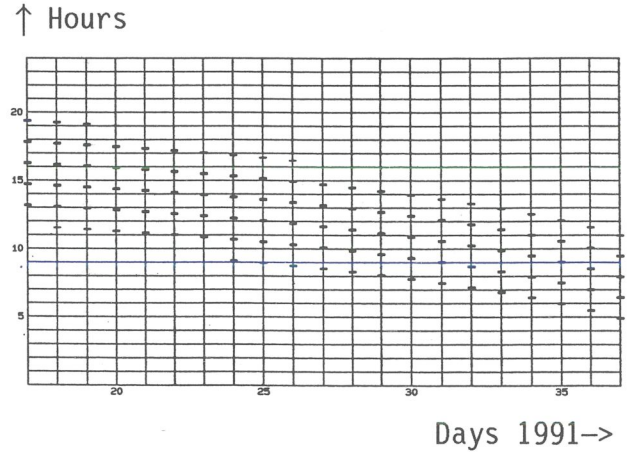


Fig. 1.2.2: Observation intervals 17 Jan.- 6 Feb. 91 of SALYUT-7/KOSMOS-1686, computed for the FGAN-FHP radar at Wachtberg-Werthhoven.

## 2. 34-m-ANTENNA AND TRACKING RADAR

### 2.1 34-m-Antenna

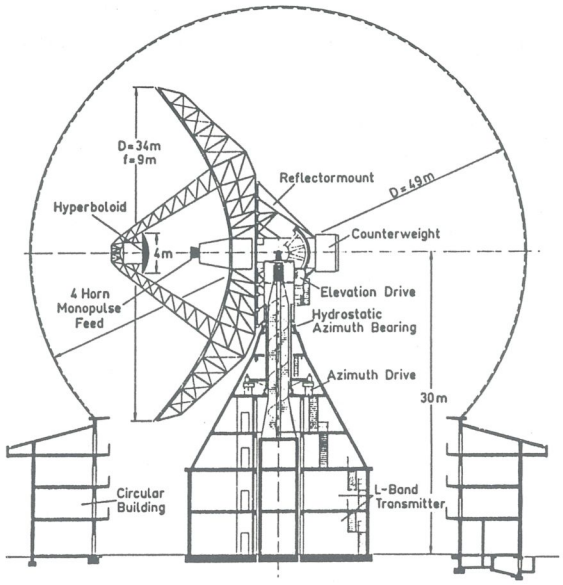


Fig. 2.1.1: 34-m-antenna at Wachtberg-Werthhoven.

The core of the experimental radar system is a highly engineered fully computer controlled elevation-over-azimuth pedestal mount (Fig. 2.1.1). It supports a 34-meter diameter parabolic reflector. The feed arrangement is based on the Cassegrain principle. The instrument is shielded from atmospheric influences by a rigid radome with 49-meter diameter.

### 2.2 Tracking Radar

Typically the L-band tracking radar transmits pulses with a pulse length of 1 ms using a 4-horn monopulse feed. The signal processing concept is designed to be fully coherent. It is based on modern correlation techniques supporting pulse compression. The following radar data are gained with the pulse repetition frequency (PRF): target direction (azimuth and elevation angles), slant range, Doppler frequency, echo signal amplitude and phase. In addition the time, the transmitted pulse power, and weather data (temperature, relative humidity, and air pressure) to cope with tropospheric refraction are measured.

### 2.3 Narrowband Radar Signature

Fig. 2.3.1 shows a typical L-band radar measurement protocol: The narrowband signature-time-plot, the observation scenario in a polar plot ("x" marks the start of measurement, "*" the CPA), and the development of range and range rate data. In addition a set of mean orbital elements (Brouwer) computed from radar data and data to identify the CPA are presented.

The data were measured after SALYUT-7/KOSMOS-1686 had lost its gravity gradient stabilization and performed a slow complex rotation. The rotation period was much longer than the observation interval. It is evident, that only using these narrowband signatures the space station attitude can not be derived.

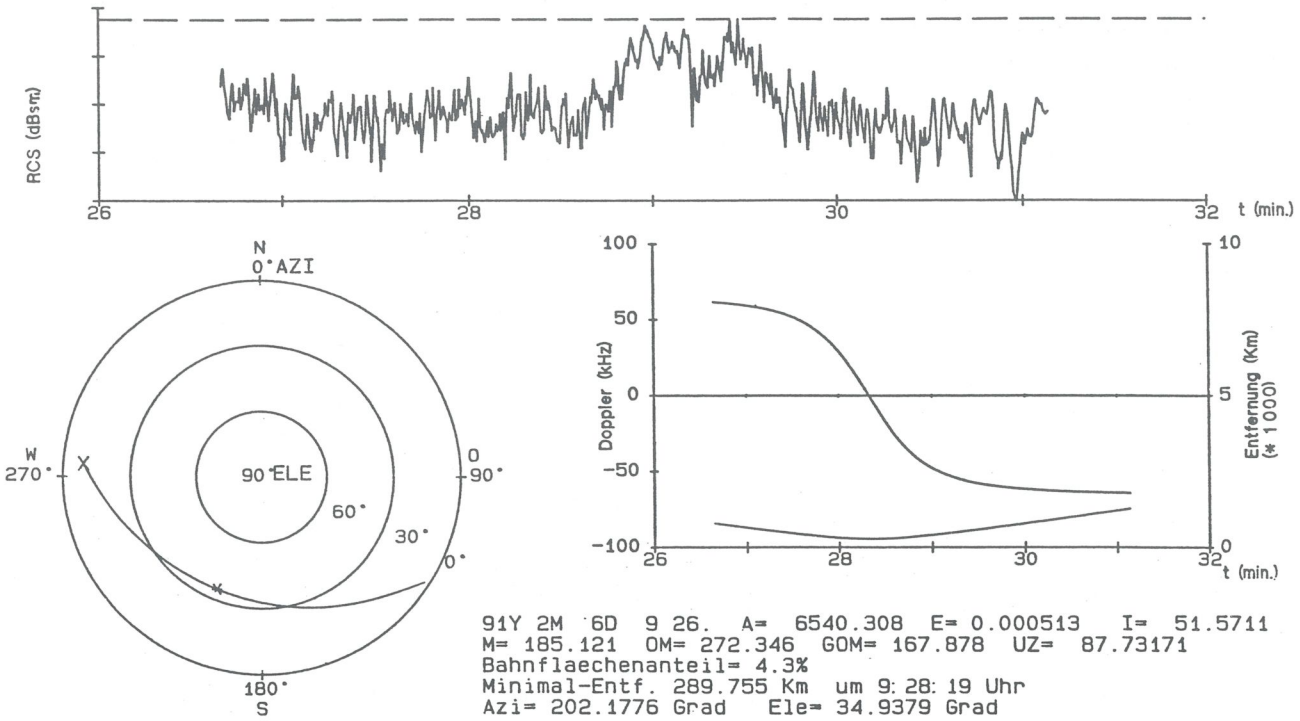


Fig. 2.3.1: Typical narrowband signature of SALYUT-7/KOSMOS-1686, slow complex rotation, 6 Feb. 91, 9:26 UTC.

## 3. IMAGING RADAR

### 3.1 Concept of Signal Processing

The Ku-band imaging radar is a fully coherent high resolution radar, operating simultaneously but not synchronized with the L-band radar on the same target. The bandwidth is generated by linear, frequency modulated (LFM) impulses. The Ku-band radar range-gate is computer controlled using L-band radar data. The signal processing concept makes use of the de-ramp technique. Ku-band radar data gained with PRF are: 1024 complex samples of the echo signal, transmitted pulse power, and time. Fig. 3.1.1 shows a simplified block diagram of the signal processing concept.

### 3.2 Range-Doppler Imaging (RDI)

The task of an appropriate radar-imaging system is the assessment of the spatial distribution of a collection of scattering centres (specular glint points or lines) which make up the target of interest. The expected result of the imaging process will be a two-dimensional representation (like a photo) of the projection of the scattering centre distribution. A well-established method which achieves this requirement and which is used by FGAN-FHP is the range-Doppler imaging (RDI) approach, or equivalent in meaning: the inverse synthetic aperture radar (ISAR) (Ref. 1-4).

3.2.1 Range-Doppler turntable imaging. In order to sketch the principle of RDI the initial turntable situation is shown in Fig. 3.2.1: a target is rotating in a xyz-coordinate system with the constant angular velocity vector $\underline{\Omega}$ pointing in z-direction and where the radar is assumed in negative y-direction.

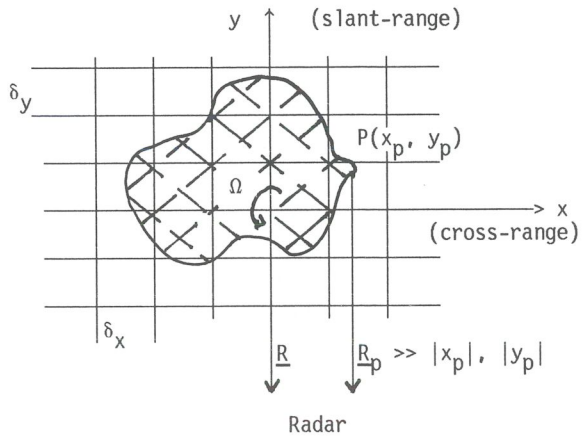


Fig. 3.2.1: Range-Doppler turntable imaging.

It can be shown by a simple evaluation of the phase of any scattering centre P that the unknown coordinates ($x_p$,$y_p$) can be assessed with aid of a two-dimensional Fourier transform. The y-coordinate can be obtained by a delay measurement, i.e. by making use of the radar signal bandwidth B. In order to determine the orthogonal x-coordinate, a synthetic aperture with an aperture angle $\Delta\varphi$ must be generated,

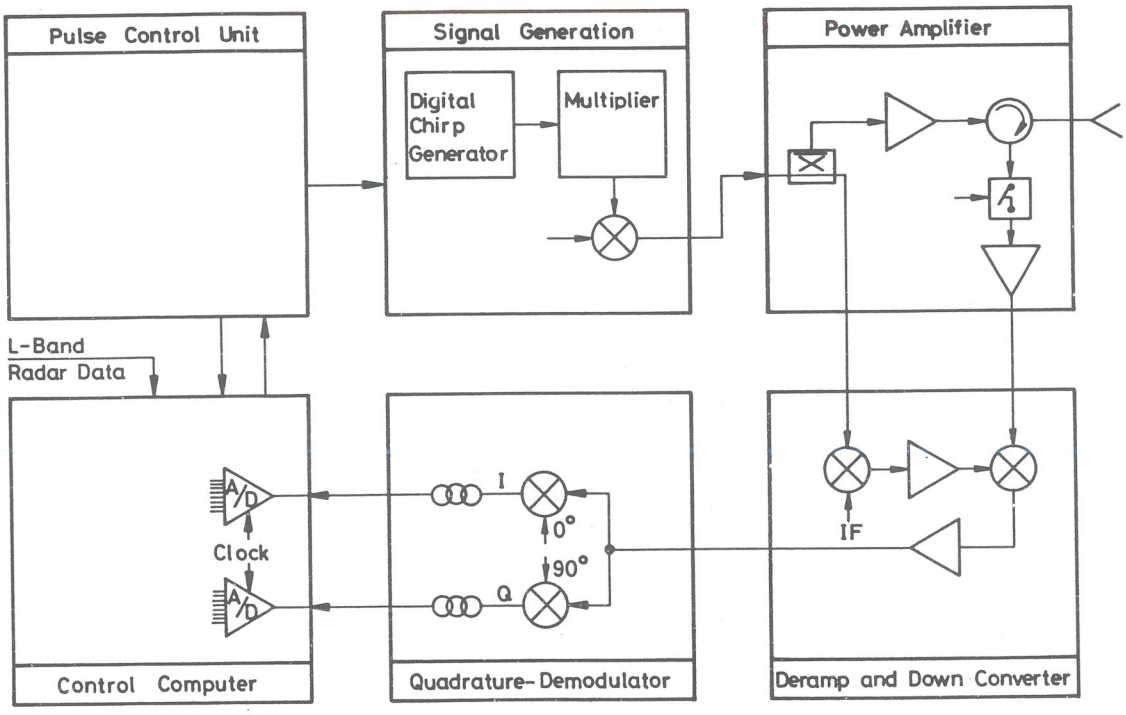


Fig. 3.1.1: Simplified block diagram of the imaging radar.

i.e. a relative rotation between the object and the radar is required. This is the principle of the synthetic-aperture radar (SAR), where it doesn't make any difference, how the effective rotation takes place. It should be emphazised that RDI (or ISAR) requires no more and no less than a change of the aspect angle between the radar and the target, whereas any range change is damaging to the imaging process and must be compensated for.

The range-Doppler analysis of the radar echoes yields a radar image of the scattering centre locations in a projection plane, which is identical with the plane of rotation (the xy-plane in Fig. 3.2.1). The longitudinal (y) axis is parallel to the observation vector $\underline{R}$, and the lateral (x) axis is parallel to the cross-product ($\underline{\Omega} \times \underline{R}$). The range-Doppler image is the convolution of the projected scattering centre distribution with the point-spread function (PSF) which is the radar image of a point object.

A figure of merit of the imaging process is the 3-dB resolution (Eqs. 3.2.1-3.2.2), i.e. the 3-dB beamwidth of the PSF in range (x) and cross-range (y):

$$\delta_x = p \cdot \lambda/(2 \cdot \Delta\varphi); \qquad (3.2.1)$$

$$\delta_y = p \cdot \lambda/(2 \cdot B_r); \qquad (3.2.2)$$

where: $p$ window factor,
$\lambda$ wavelength of radar signal,
$f$ frequency of radar signal,
$B_r = B/f$ relative bandwidth of radar signal,
$\Delta\varphi$ synthetic aperture angle.

It turns out that both resolutions, range and cross-range, are independent of range. This highly important fact as well as the night-and-day and all-weather capability of radar make RDI a valuable tool for long-range non-cooperative target identification.

3.2.2 Principles of RDI processing with target motion. However, if one would like to make use of these nice properties of RDI in real life, i.e. in the dynamic flight situation of noncooperative targets, one has to get over the main hindrance: the restriction of RDI on the stationary turntable situation. How this can be achieved will be discussed during the course of the following short description of the principle of RDI-processing, which is sketched in a flowchart in Fig.3.2.2.

RDI processing starts with the received and deramped radar echoes which have to be compressed in slant-range in a first important step comprising: calibration, compensation for system errors and residual chirp, windowing, and FFT. The result is a collection of slant-range profiles which are jittering in slant-range direction because of the limited accuracy of range-gate tracking.

In a next step, the most important one, the stationary turntable situation must be established, which belongs in Fig. 3.2.2 under the headword "data centring":

- Firstly, the coherent processing interval $\Delta t$ has to be assessed, which means the estimation of the intrinsic motion of the target. Usually, this is not a problem in the case of attitude stabilized or simply rotating satellites, but problems might result in cases of satellites with a complex rotational motion.
- Secondly, the jittering slant-range profiles have to be aligned. This is attained by a correlation method using a range profile replica function which can remember previous range profiles.
- Thirdly, the time dependent range phase, which is a consequence of the translational motion component has to be compensated for. This can be done in a great variety of different ways, where autofocussing methods turn out to be the most versatile approaches.

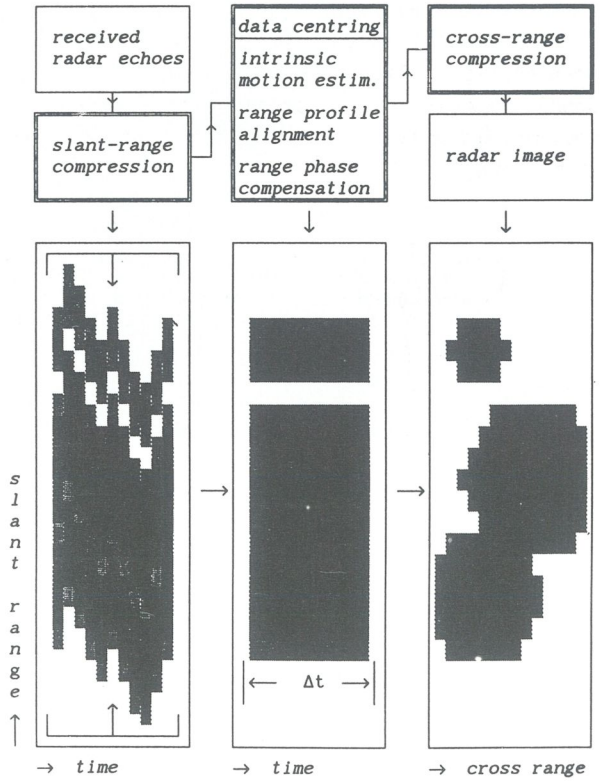


Fig. 3.2.2: Principles of RDI processing

The result of this data centring approach is a two-dimensional range profile matrix which contains in its columns the aligned and range-phase compensated range profiles.

In a final step the cross-range compression of the centred range profiles yields the desired radar image, i.e. the projection of the visible scattering centres onto the instantaneous rotation plane, where the x- and y-coordinates are defined as in Fig. 3.2.1.

## 4. RADAR IMAGING OF SALYUT-7/KOSMOS-1686

Many passages of SALYUT-7/KOSMOS-1686 have been observed with the FGAN-FHP imaging radar since January 1990 in order to monitor possible changes in the attitude and the condition of the space station which is shown on a photo in Fig. 4.1. Because of the lack of other recent pictures of SALYUT-7/KOSMOS-1686 this snap which was shot from a soviet video (Ref. 5) was chosen. The video was taken from the departing SOYUZ-T15 crew after having mothballed the space station in 1986. Despite the bad print quality the tandem configuration of both space vehicles can be clearly identified and differences in the solar panel structure are evident.

Fig. 4.1: SALYUT-7/KOSMOS-1686 taken from the departing SOYUZ-T15 crew; (Spaceflight, Feb. 1989, Ref. 5).

A typical radar image from the first observed track on 23 January 1990 is shown in Fig. 4.2 where a particular flight situation is chosen: the closest point of approach (CPA, $\dot{R}$=0 km/s) at the rather high elevation of E=80°. Several data of interest are noted in the bottom line in each radar image: The NASA catalog number, the aspect angle (the angle between the velocity vector $\underline{v}$ and the observation vector $\underline{R}$), and the data and time (UTC) (year, day, hour, minute, and second).

In the radar image in Fig. 4.2 both docked satellites with the different solar panel structures can be easily distinguished, where KOSMOS-1686 is the object near to the earth. As can be seen from Fig. 4.2 as well, there is a slight tilt of the longitudinal axis with respect to the radar LOS. From analysis of this and other radar images it was found out that the space station was gravity gradient stabilized at that time with the longitudinal axis executing slow oscillating rotatory motions around the local vertical. The observed half-cone angle was less than 20°.

This gravity gradient stabilized attitude of the space station didn't change until 17 January 1991. On 21 January 1991 a clearly recognizable attitude change was monitored from the radar images for the first time and all subsequent radar images indicated that the space station was executing now a slow complex rotation.

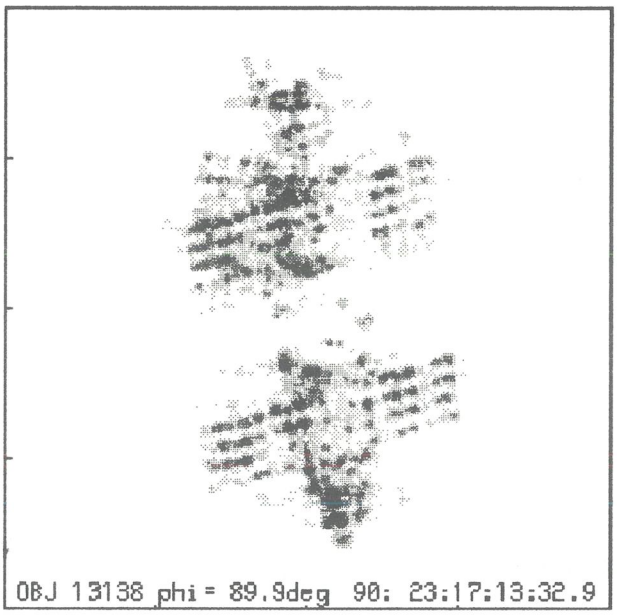


Fig. 4.2: Radar image of SALYUT-7/KOSMOS-1686, 23 Jan. 1990, gravity gradient stabilized, CPA, elevation E = 80°, range R = 418 km, range rate $\dot{R}$ = 0 km/s.

A qualitative survey over the time history of the space station's attitude is given in a sequence of radar images in Fig. 4.3. For comparative purposes all radar images have been reconstructed at rather high elevations (>= 60°) and at the CPA. The first four images (start: upper row, left image) show the space station in the gravity gradient attitude whereas the remaining images clearly reveal the rotational motion. In some of these radar images the tilt of the solar panels of SALYUT-7 with respect to the longitudinal axis becomes evident.

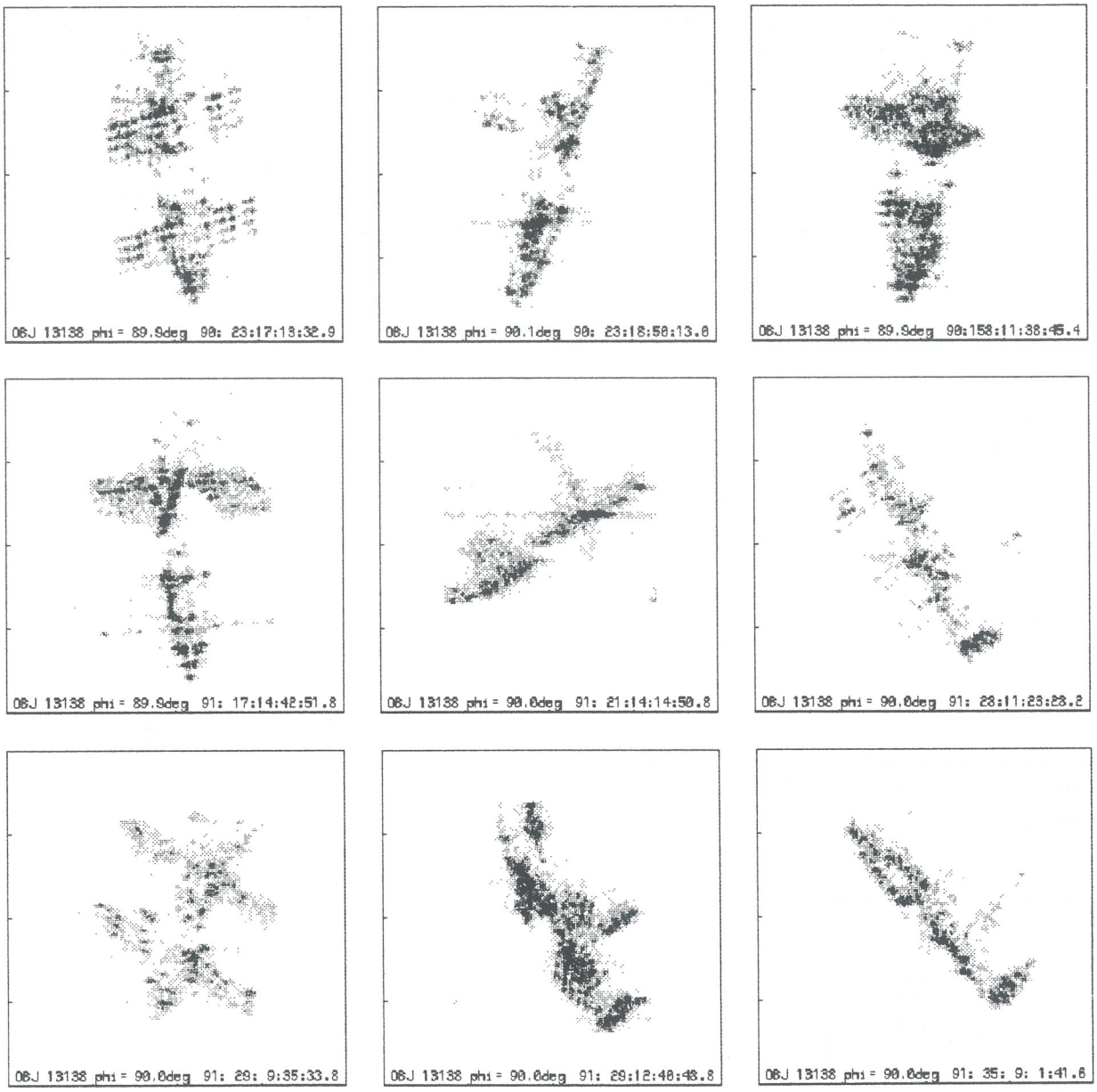


Fig. 4.3: Sequence of radar images of SALYUT-7/KOSMOS-1686, observation period: 23 Jan. 1990 until 6 Feb. 91, elevation $E \geq 60°$, $\dot{R} = 0$ km/s (CPA).

Fig. 4.4 shows a radar image of the last passage of Salyut-7/Kosmos-1686 on 6 February 1991, which could be monitored by the FGAN-FHP radars. The most important facts which can be recognized are: The space station complex Salyut-7/Kosmos-1686 is still docked at that time but there seem to be damages to the solar panel structure of Salyut-7 (one solar panel appears to be bent).

## 4. CONCLUSION

Radar observations of non-cooperative high risk space objects during reentry provide reliable information. Narrowband tracking data are used to predict the actual orbit, to assess the lifetime and risk, and to compute position of subtracks for the decay-time-window. High resolution radar data are essential to compute radar images. Assessments about size, shape, attitude, and information about disintegration or major changes of the satellite structure are gained from the radar images. At FGAN-FHP the availability of radar data and the reliability

of analysis methods and results were demonstrated during the reentry of the USSR space station SALYUT-7/KOSMOS-1686.

As in other major reentry campaigns (KOSMOS-954, SKYLAB-1, KOSMOS-1402, KOSMOS-1900) FGAN-FHP supported and advised the German government in all matters concerned with the decay.

It was the first time that FGAN-FHP provided ESA-ESOC timely and frequently with tracking radar data, state vectors computed from radar data, and analysis results (orbital lifetime, attitude behaviour, deformation of space station structure) during the entire reentry-campaign of SALYUT-7/KOSMOS-1686. The radar data were: azimuth, elevation, range, range rate, and time. The elevation and range data were corrected from tropospheric refraction effects before transmitting them to ESA-ESOC.

The information provided from FGAN-FHP enabled ESA-ESOC to perform reentry computations and risk assessments on their own and to inform ESA-Member-States (not being able to do reentry predictions) on all matters of the decay.

It is evident to all parties concerned with reentry problems that the availability of data are the crucial point.

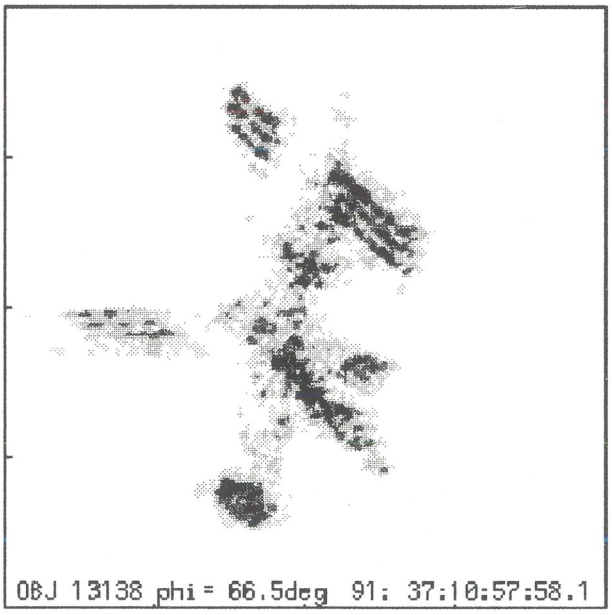


Fig. 4.4: Radar image of SALYUT-7/KOSMOS-1686, 4 Feb. 1991, complex rotation, elevation E = 3.4°, range R = 1160 km, range rate $\dot{R}$ = -3 km/s.

## 6. REFERENCES

1. J. L. Walker 1980, Range-Doppler imaging of rotating objects, IEEE Trans. AES-16, pp.23-52.

2. D. A. Ausherman, A. Kozma, J. L. Walker, H. M. Jones, E. C. Poggio 1984, Developments in radar imaging, IEEE Trans. AES-20, pp. 363-400.

3. D. R. Wehner 1987, High resolution radar, Artech House, Norwood.

4. D. L. Mensa 1991, High resolution radar cross-section imaging, Artech House, Norwood.

5. N. Kidger 1989, Soviet spacecraft revealed, Spaceflight, 31 (Feb. 1989), p. 56.